Preliminary LIDAR Data Report

James Churnside, Richard Marchbanks, NOAA ESRL, May, 2012

Abstract: The NOAA LIDAR was flown in coordination with the R/V *McArthur II* to survey small pelagics in the northern Gulf of Mexico in Late September and early October, 2011. This report describes preliminary results from the lidar data. The LIDAR was able to penetrate to > 30 m in offshore waters and 20 – 30 m on the shelf, except for the Mississippi River plume, where penetration was < 20 m. Few dense schools were detected, and those were generally found on the shelf. Several of these were positively identified as aggregations of moon jellies (*Aurelia sp.*). Large numbers of single targets were detected, especially off the shelf. Generally, more schools and single targets were detected at night than during the day, suggesting diurnal migration. Other features, including large layers and plumes were also observed. The layers are probably phytoplankton, but some of the plume structures might be oil from seeps. Comparison with the data from the surface vessel will be used in the final analysis to confirm the identity of the features detected by the LIDAR.

1   INTRODUCTION

Oil released from the broken Deepwater Horizon well head both dispersed at depth and rose through nearly a mile of water column. The composition of the released gas-liquid mixture changed over time and space as the result of dilution, changes in pressure, dissolution, and addition of other constituents such as dispersants, methanol, and anti-foaming additives. Of oil that made it to the water surface, some entrained water forming mousse, some was dispersed into the water column naturally and by application of dispersants, and some was removed mechanically or by *in situ* burning. Floating oil, oil droplets, flocculated and dissolved components were transported large distances at various levels of the water column. Oil also picked up sediments, and other particulate material, some of which became neutrally or slightly negative buoyant, sinking to various depths. The oil dispersed at the wellhead (both via turbulence or by injection of dispersants) was transported by currents that varied in time and space, yielding a complex pathway of subsurface oil contamination that affected abyssal, bathypelagic, and meso-pelagic waters of the offshore Gulf of Mexico.

Fish and invertebrates in the water column are exposed to contaminants by swimming through contaminated water, spending time on/in contaminated sediments, taking up contaminants through body surfaces, passing contaminated water over respiratory structures, and ingesting water, oil droplets, contaminated biota, and particulates contaminated with oil as part of feeding. Additionally, sensitive life stages of pelagic fish and invertebrates come in direct contact with floating oil that covers and is mixed into the neuston layer (upper ~0.5m) where many embryos and larvae develop. Other neustonic organisms exposed to surface oil include many small invertebrates important to the food web. In the water column, organisms are also exposed to suspended oil droplets, which can foul appendages or other body surfaces. Water column organisms have also been exposed to dispersants dissolved in water, on oil droplets and adsorbed to suspended particulate matter. Water column organisms were

also exposed to dissolved and water-borne chemical additives such as methanol and anti-foaming agents. Small pelagic fish and other epipelagic biota in the surface waters of the north-eastern Gulf of Mexico are among those biota potentially exposed to the released oil and spill-related chemicals.

Small pelagic fish are important components of the marine food web, consuming plankton and providing food to predators including large pelagic fish (e.g., tuna, billfish, etc.). Limited information is available on the abundance and distribution of schooling pelagics and other difficult-to-sample organisms in near surface waters of the northern Gulf of Mexico. Because this epipelagic habitat may have been impacted by response activities and contaminants during the course of the DWHOS, additional data regarding small pelagics in this habitat are needed for the damage assessment.

Net sampling gear deployed during the course of the NRDA study may not efficiently sample the more mobile biota of the epipelagic environment due to gear avoidance behavior. Similarly, most of the acoustic surveys relied on hull mounted transducers which may have missed the upper few meters of the water column. One method for acquiring relevant data is through the use of airborne LIDAR (LIght Detection And Ranging). LIDAR is similar to RADAR or acoustics in that energy is propagated through the environment and returned in the form of backscatter from a target, but the energy source in LIDAR is a brief pulse of laser light. Airborne LIDAR is a well-established technology and has the additional benefit that a given area can be surveyed rapidly and repeatedly with minimal gear avoidance problems.

NOAA has been deploying a LIDAR system (NOAA Fish LIDAR) for approximately 10 years to measure distributions of epipelagic fish schools and plankton layers. This LIDAR, with some changes in the configuration, has been used in numerous investigations of pelagic fish distributions, including sardines and anchovy off the US west coast (Churnside and Wilson 2001; Churnside, Demer et al. 2009; Reese, O'Malley et al. 2011), capelin in the Gulf of Alaska (Brown, Churnside et al. 2002), mullet and other pelagics in the eastern Gulf of Mexico (Churnside, Demer et al. 2003), salmon in the Gulf of Alaska (Churnside and Wilson 2004), juveniles of a number of species in the Atlantic off southern Europe (Carrera, Churnside et al. 2006), mackerel in the Norwegian Sea (Tenningen, Churnside et al. 2006; Churnside, Tenningen et al. 2009), and menhaden in Chesapeake Bay (Churnside, Sharov et al. 2011). It has also been used in investigations of zooplankton (Brown, Churnside et al. 2002; Churnside and Thorne 2005) and phytoplankton (Churnside and Donaghay 2009).

Given the utility of this instrumentation and the specific problem that it can address, airborne LIDAR surveys in the northern Gulf of Mexico were performed in coordination with a ship-board (R/V *McArthur II*) sampling program to ground truth the LIDAR measurements. Data returned from this program will help the NRDA estimate the distributions and abundances of schooling pelagic and other organisms (i.e., herring, sardine, menhaden, bumper, flyingfish, anchovies, silversides, shad, scad, mullet, butterfish, and harvestfish, as well as gelatinous organisms) inhabiting the epipelagic environment from the surface to approximately 20-50 meters. This report describes preliminary results of the LIDAR data before the comparison with the surface data.

1.1 Objectives

This report, covering a portion of the NRDA Late-Summer 2011 Small Pelagics survey, describes the NRDA survey for September-early October 2011 in which a subset of the SEAMAP stations, and transits/transects between them, were selected for sampling of epipelagic organisms (juvenile and adult small pelagic fish and gelatinous zooplankton) in the surface waters of the northern Gulf of Mexico potentially affected by the DWHOS and in surrounding areas.

There were five specific objectives described in the work plan:

a. Document the large scale distribution of epipelagic fish and plankton in the study area. Large scale aerial surveys corresponding to, and extending beyond, ship cruise station and tracks will be performed. This will allow us to document the distribution of epipelagic organisms and identify spatio-temporal changes that may be associated with hydrographic variability, the passage of weather fronts, etc.

b. Document day/night differences in the distribution of fish and plankton. Selected regions will be surveyed during the day and again the same night. Diel vertical migration has been a particular focus of some of the NRDA cruises and this effort will afford additional insights into that process more synoptically than can be accomplished with ship-board surveys.

c. Investigate spatial scales not available to the ship survey. Ship surveys are often a compromise between covering a large enough area and covering an area with sufficient spatial resolution. Aerial surveys can extend beyond the area of ship surveys to ensure that most of the biological concentrations are captured and can also cover some areas with finer resolution to ensure that small-scale processes are captured.

d. Use aerial imagery/LIDAR to direct ship sampling to regions of high biological concentrations. The aerial surveys can easily detect biological hot spots that may be missed by a ship survey. These areas may be located beyond the planned extent of the ship survey or may be located between survey stations or transects. They may even be directly on a surface-transect but occur before or after the ship passes. Any hot spots will be intensively investigated by the aircraft, and the Chief Scientist on the ship notified of its position. If the ship is in the area and can be feasibly redirected to the hot spot identified by the aircraft, the ship will sample in the area of interest for ground truth measurements if logistics allow.

e. Collect biological, physical, and acoustic data aboard the *McArthur II* to help support and interpret the LIDAR observations.

This report describes the results of the LIDAR portion of the investigation. The next step in the analysis will be to compare these results with the data from the surface vessel. This information should allow us to better identify sources of the LIDAR returns. Ideally, this identification would be done to the species level, but this may not be possible in all cases. Later, the LIDAR and surface data will be jointly analyzed, along with environmental data, to attempt to understand the observed patterns.

2   MATERIALS AND METHODS

2.1   Airborne LIDAR

The NOAA Fish LIDAR was installed on a small (King Air 90) twin-engine aircraft, which was deployed to Stennis International Airport, Mississippi. The LIDAR system is a non-scanning, radiometric LIDAR that is similar in principle to a vertical echosounder. A block diagram is presented in Figure 1. The major components were 1) the laser and beam-control optics, 2) the receiver optics and detector, and 3) the data collection and display computer. The system also includes the capability to record time, aircraft position, and system parameters (e.g., receiver gains). It was flown at a nominal altitude of 300 m and speed of 80-100 m s^{-1}.
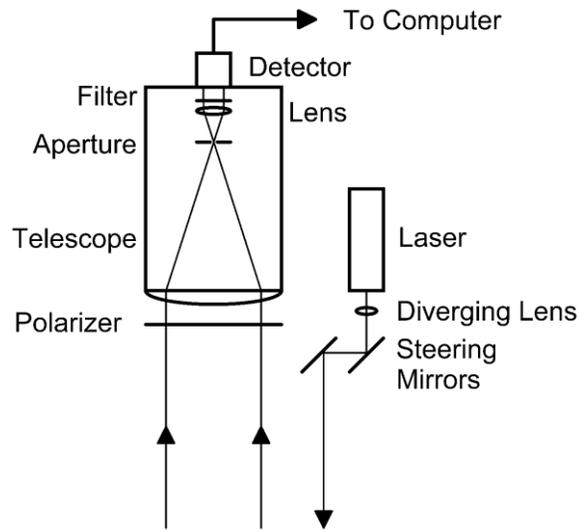
Figure 1. Schematic diagram of LIDAR system, showing the laser transmitter and one of two receiver telescope assemblies.

The laser is a frequency-doubled, Q-switched Nd:YAG laser that produces about 100 mJ of green (532 nm) light in a 12-nsec pulse at a rate of 30 pulses per second. The laser is linearly polarized. The beam from the laser is diverged, with a lens in front of the laser, to produce a 5 m diameter spot on the surface. At this size, the irradiance at the surface is safe for human observers and also for marine mammals. (Zorn, Churnside et al. 2000). Two steering mirrors allow the transmitted beam to be aligned with the receiver telescopes.

Two receiver channels were used – one with a polarization filter parallel to the laser polarization and one with a filter oriented to pass the orthogonal polarization. Each telescope collects the light onto an interference filter to reject background light. An aperture at the focus of the primary lens also limits background light by limiting the field of view of the telescope to match the divergence of the transmitted laser beam. The filtered light is incident on a photomultiplier tube, where it is converted into an electrical signal. Other than filter orientation, the only difference between the two receiver channels is telescope diameter. The return that is co-polarized with the transmitter is larger, so this telescope is smaller (6 cm diameter) than the cross-polarized channel (15 cm diameter). The

photomultiplier tube outputs are fed into an amplifier with a logarithmic response to increase dynamic range to 80 dB and digitized at 10^9 samples per second. This sample rate produces a depth resolution of about 11 cm in water.

The data were collected by a dedicated computer running the LabView real time system. This is connected to a laptop through an Ethernet for control and display in real time. The raw data can be displayed on the aircraft as an echogram or the individual LIDAR profiles can be plotted. Schools, layers, plumes, and individual fish are all recognizable in real time with these displays.

2.2 Data Collection

The study area of interest was a region bounded by 87° W and 90.5° W and by 28° N and 30° N (Figure 2) around the vicinity of the Macondo well site. Three sampling strategies were employed. The first was a large-scale survey of the entire area along constant-longitude lines separated by 0.5°, as depicted by the gold lines in Figure 2. We planned to do this at the beginning of the campaign and again at the end. The second was a series of small-scale surveys that would each cover a region 10-20 nmi on a side with a transect spacing of about 0.75 nmi. The locations of these were to be based on hot spots located during the initial large-scale survey and by regions of interest located by the surface vessel. The final sampling strategy was a broad-area search pattern that would be implemented to find additional areas of interest. Rather than a fixed grid, this flight pattern would investigate regions of potential biological activity, such as the continental shelf break and the edge of the Mississippi River plume. Except for the search pattern, we planned to fly each of the planned patterns during the day with a repeat flight that same night to investigate diurnal variability.
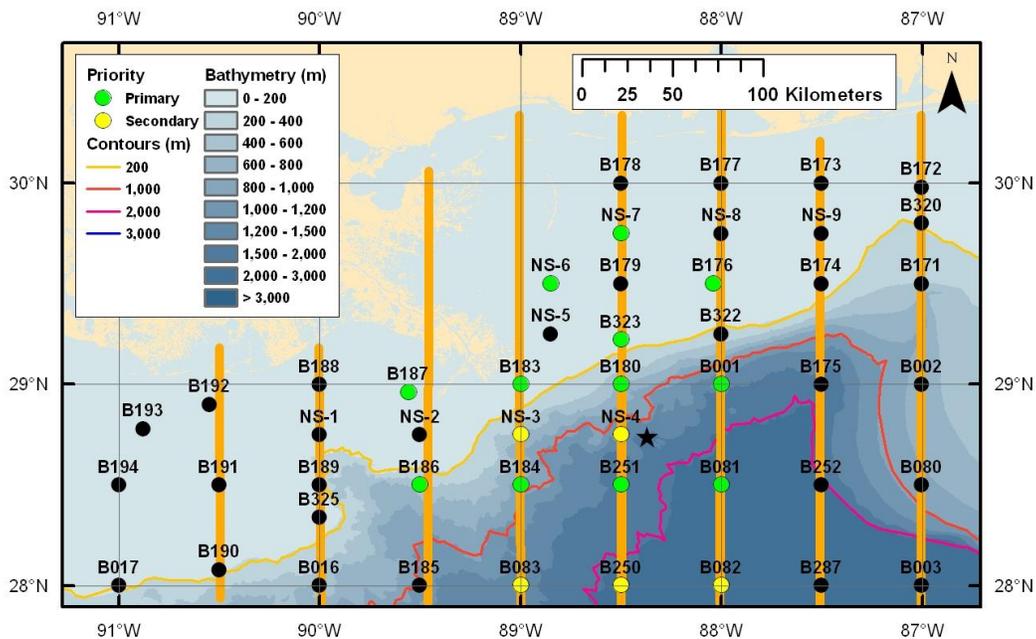
Figure 2. Chart of north-central Gulf of Mexico showing historic hydrographic stations (solid circles), primary (green) and secondary (yellow) stations planned for the R/V

McArthur II, the spill site (star), and the planned coverage of the large-scale aerial surveys (gold lines).

The resulting flight schedule is summarized in Table 1. Flights were generally made between 24 September and 8 October, 2011. Where possible, a daytime flight was followed by a nighttime flight over the same track. For our purposes, daytime and nighttime were considered to be at least one hour before sunset and at least one hour after sunset, respectively. Sunset was roughly 19:00 CDT or 0:00 UTC. The large-scale surveys were too large to be covered in a single flight, so were separated into a eastern (87° - 88.5° W) and western (89° - 90.5° W) sections.

Table 1. Summary of flights. No useful data were obtained from highlighted days.

date	day flight	night flight
24-Sep	large east	large east
25-Sep	large west	large west
26-Sep	small slope	small slope
27-Sep	none	None
28-Sep	aborted	None
29-Sep	small shelf	small shelf
30-Sep	large center	None
1-Oct	large center	large center
2-Oct	search	None
3-Oct	small offshore	small offshore
4-Oct	small shelf	small shelf
5-Oct	small slope	small slope
6-Oct	none	Aborted
7-Oct	large east	large east
8-Oct	aborted	None

The first two days were devoted to a large-scale survey of the entire study area, with repeat day and night coverage. The third day was a small-scale survey on the continental shelf break where relatively high concentrations of fish were observed during the first two days. After two days of weather delay, a small-scale survey was performed on the continental shelf. The following day, 30 September, a large-scale survey was performed in the center of the study area, where the highest concentrations of fish had been observed. The corresponding night flight was canceled because of weather, so the same survey was performed day and night the following day. On 2 October, we flew a daytime search pattern following visible fronts on the shelf and the shelf break. This was followed by three days of small-scale surveys beyond the continental shelf, on the shelf, and along the shelf break, respectively. The final successful flight repeated the eastern half of the original large-scale survey. An attempt to repeat the western half of that survey was unsuccessful, due to weather.

2.3 Data Processing

We processed the LIDAR data using visual inspection of the cross-polarized return. This channel consistently has a higher contrast between fish and the surrounding water than does the co-polarized return. A program was written in the IDL programming language that would read the raw LIDAR data in 2000-shot increments, perform some initial processing, wait for inputs from the operator, and save the results.

The initial processing was primarily to make the display easier to see. The cross polarization data were selected and the position of the surface in each shot was identified. The position changed because the distance from the aircraft to the water changed with variations in altitude and attitude. With the surface position information, the data could be displayed as a function of depth. Depths greater than 50 m were ignored as below the maximum penetration depth. The raw data were then displayed on the computer screen.

With the data displayed on the screen, the operator selected schools, individual targets, or layers manually. Schools and layers were outlined by a mouse click at the top, bottom, start, and end of each feature. Individual targets were identified with a single mouse click. In each case, the program then retrieved position, depth, length (for schools and layers), and average LIDAR scattering coefficient (for schools and single targets) of the feature, calculated the LIDAR penetration depth at that point, and saved the results. Penetration depth was defined as the depth at which the LIDAR signal dropped to within ten standard deviations of LIDAR noise level above zero. Processed data files also included the data file name and position of that feature within the file.

During the data analysis, large numbers of individual target returns were observed, and we performed additional analysis to look at differences between them. To this end, we calculated the contrast and depolarization ratio for each of these returns. The cross-polarized lidar return and the depolarization were both calculated for a region comprising one meter in depth and seven lidar pulses around each object. The contrast was defined as the maximum return in the region divided by the average over the region. The depolarization was similarly calculated as the maximum depolarization divided by the average for each region. By calculating the depolarization ration in this way, we remove possible effects of the depolarization induced by multiple scattering in the water column (Churnside 2008).

3 RESULTS

The data were processed independently to obtain the distributions of fish schools, single targets, and layers. These are described in the sections below.

3.1 Fish Schools

Fish schools were identified manually in the LIDAR data, and the characteristics of each written to a text file. The positions of these schools are presented in Figures 3-5. As these charts show, we did not see high concentrations of dense schools. Most of the schools were detected on the shelf, and almost none were detected beyond the shelf break during the day. A notable exception to this is a line of "schools" near the Deepwater Horizon position. The characteristics of these returns suggest that they are

aggregations of zooplankton rather than fish. They are included in the data set so we can get confirmation from the surface data. At night, there were a few schools beyond the shelf break, suggesting possible diurnal migration.
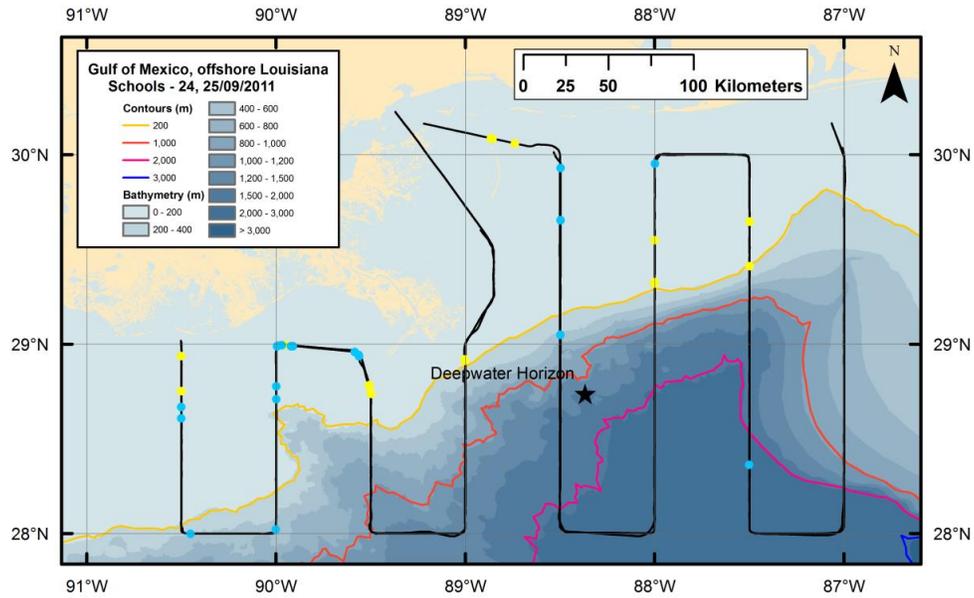
Figure 3. Flight tracks (black lines) and positions of fish schools detected during the day (yellow circles) and at night (blue circles), all from the initial large-scale survey.
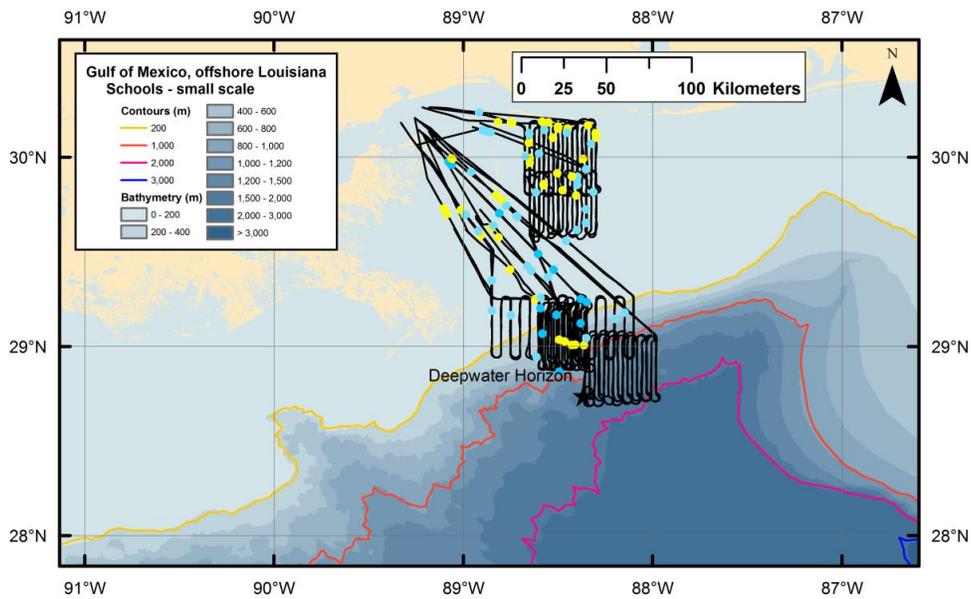
Figure 4. Flight tracks (black lines) and positions of fish schools detected during the day (yellow circles) and at night (blue circles), all from the five small-scale surveys.
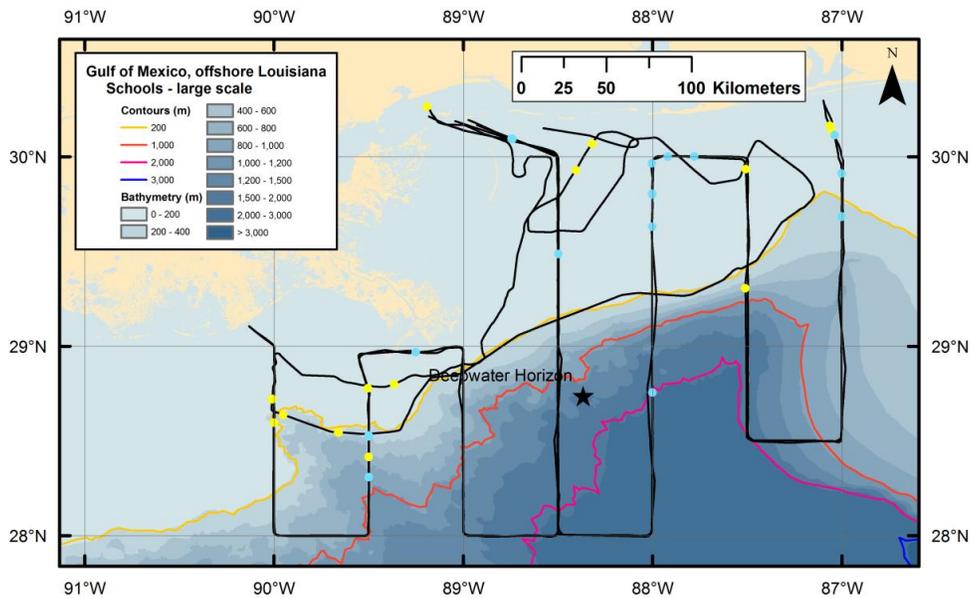
Figure 5. Flight tracks (black lines) and positions of fish schools detected during the day (yellow circles) and at night (blue circles), all from the large-scale surveys after the first one and from the search flight.

The detected schools were of several different types. One (Figure 6) is a group of small, dense schools. This pattern is typical of fish like anchovy, which we have observed in this type of configuration in shallow water off the US west coast. Another (Figure 7) is a hollow pattern of LIDAR return is similar to that produced by moon jellies (*Aurelia sp.*) during a LIDAR survey in the Pacific Northwest. This is such a distinctive pattern that we are confident in the identification, even without confirmation from the surface data. The string of daytime schools near the location of the Deepwater Horizon in Figure 4 is of a different type – very weak, isolated, and deeper.
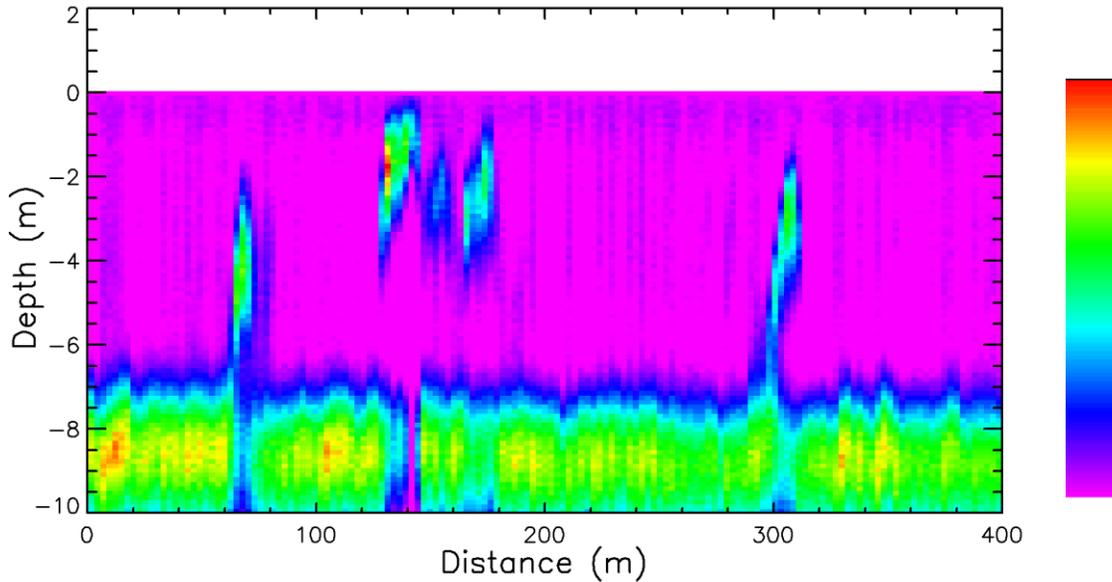
Figure 6. Collection of small, dense schools detected during the day on 24 September. These were very close to the shore; band of high return at 8.5 – 9 m is the sea floor. Colors represent the strength of the return, according to the color bar at the right. This same relative scale is used for all images, but the absolute value is adjusted to the peak.
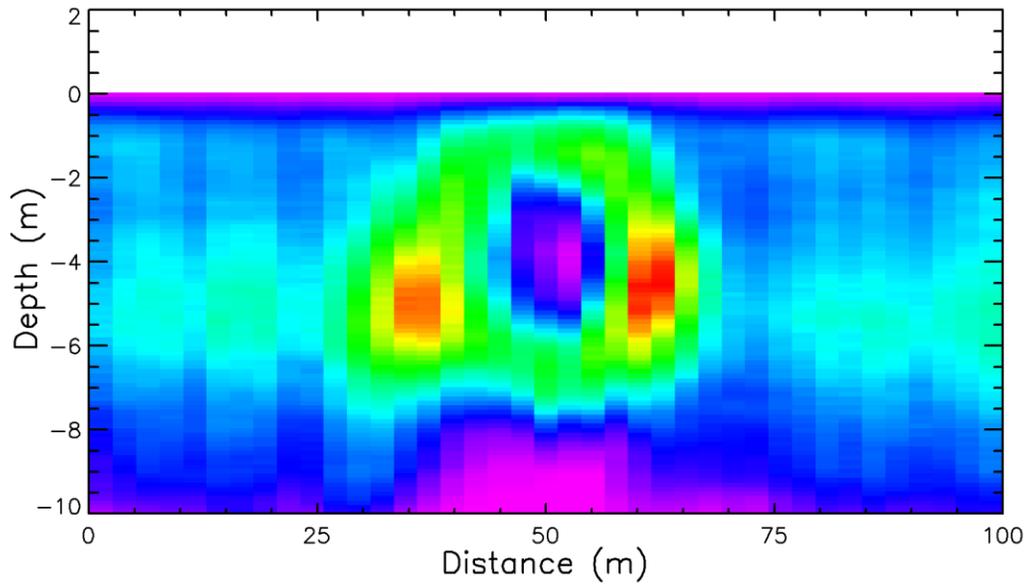
Figure 7. Hollow aggregation detected at night on 26 September.

3.2   Single Fish

There were many more single fish returns than dense schools. For our purposes, a single fish is defined as a scattering object that is smaller than our beam, but still produces a strong, cross-polarized LIDAR return. These often came in groups, as in Figure 8.
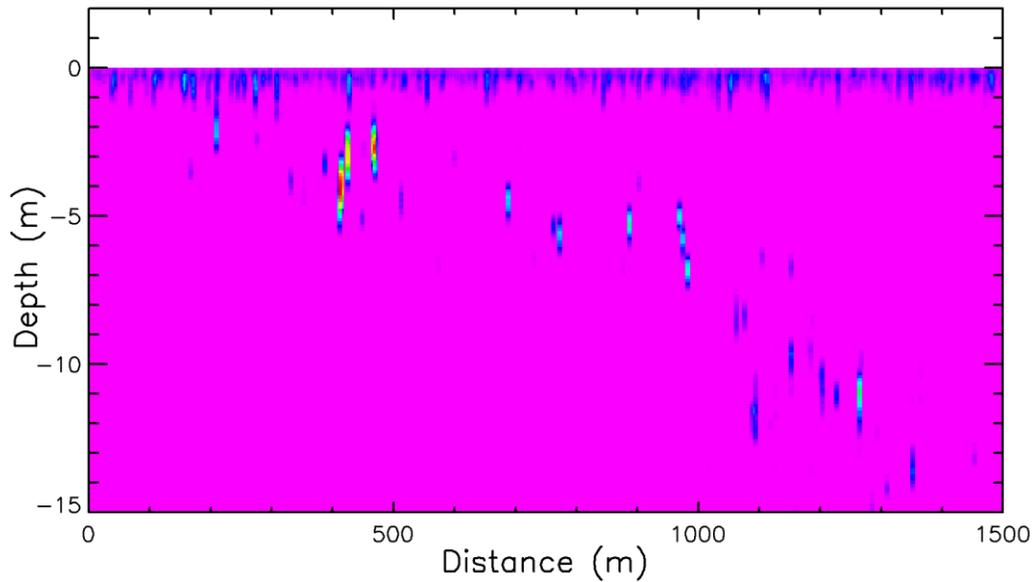
Figure 8.   Collection of single scattering objects detected during the day on 24 September.

11

The charts (Figures 9-14) show very high numbers of single fish returns. Unlike the pattern we saw with schools, there were more single fish detected in deeper water than on the shelf, especially at night. The interesting exception to this was the search flight, which detected large numbers of single fish. These animals seem to have a preference for the type of frontal features that we were following, although this needs further investigation in conjunction with the data from the surface vessel.
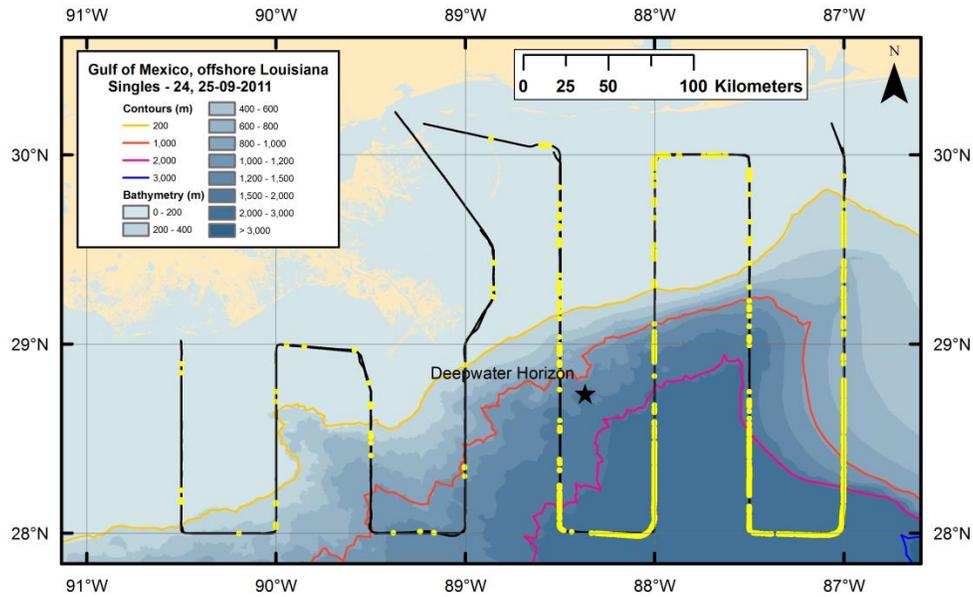
Figure 9. Flight tracks (black lines) and positions of single fish detected during the day (yellow circles), all from the initial large-scale survey.
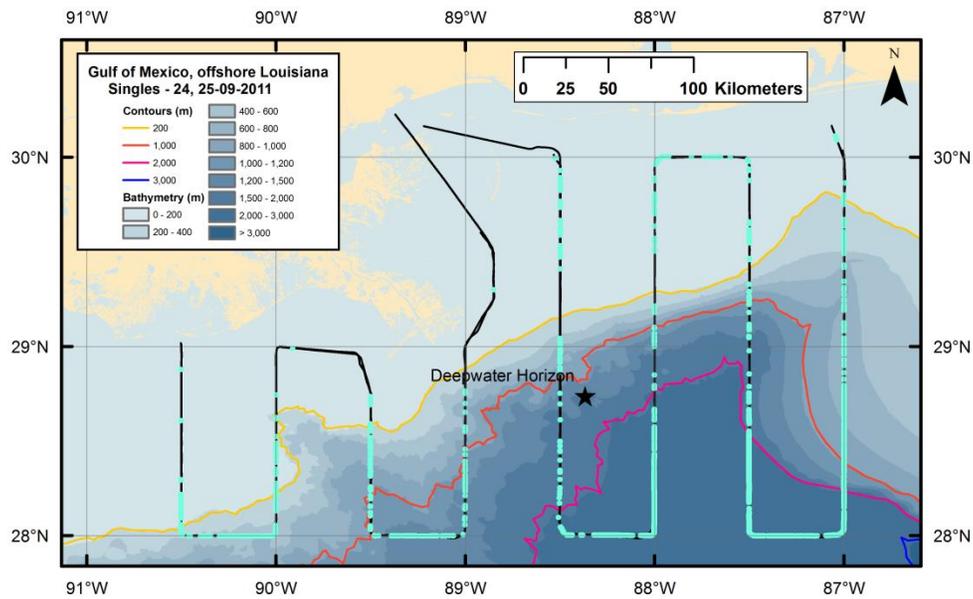
Figure 10. Flight tracks (black lines) and positions of single fish detected at night (blue circles), all from the initial large-scale survey.
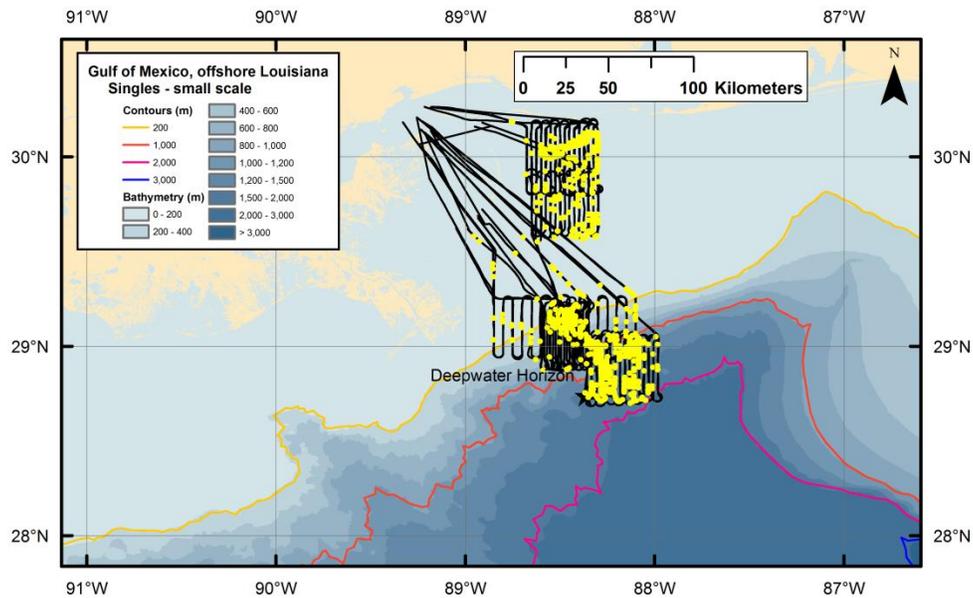
Figure 11. Flight tracks (black lines) and positions of single fish detected during the day (yellow circles), all from the five small-scale surveys.

13
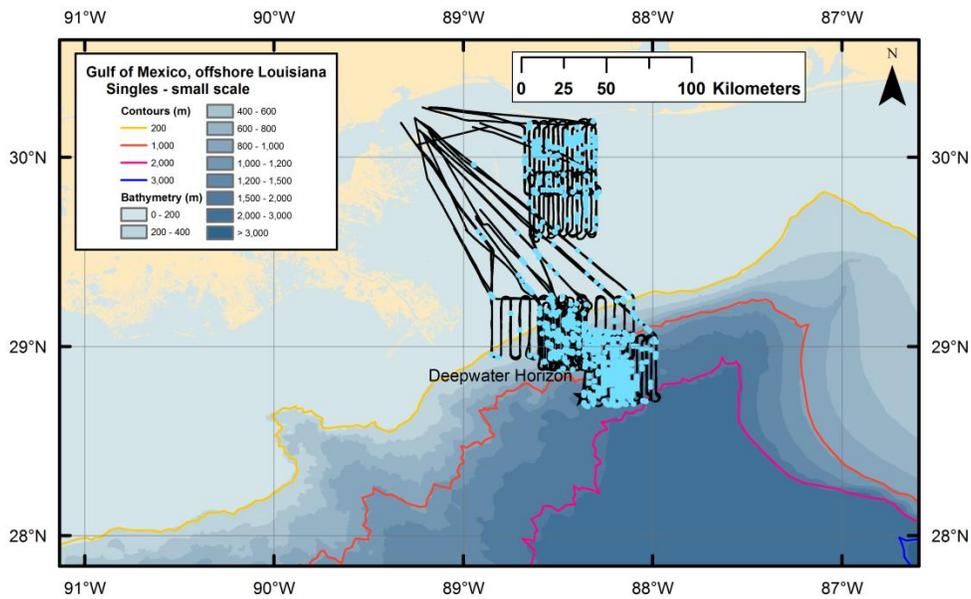
Figure 12. Flight tracks (black lines) and positions of single fish detected at night (blue circles), all from the five small-scale surveys.
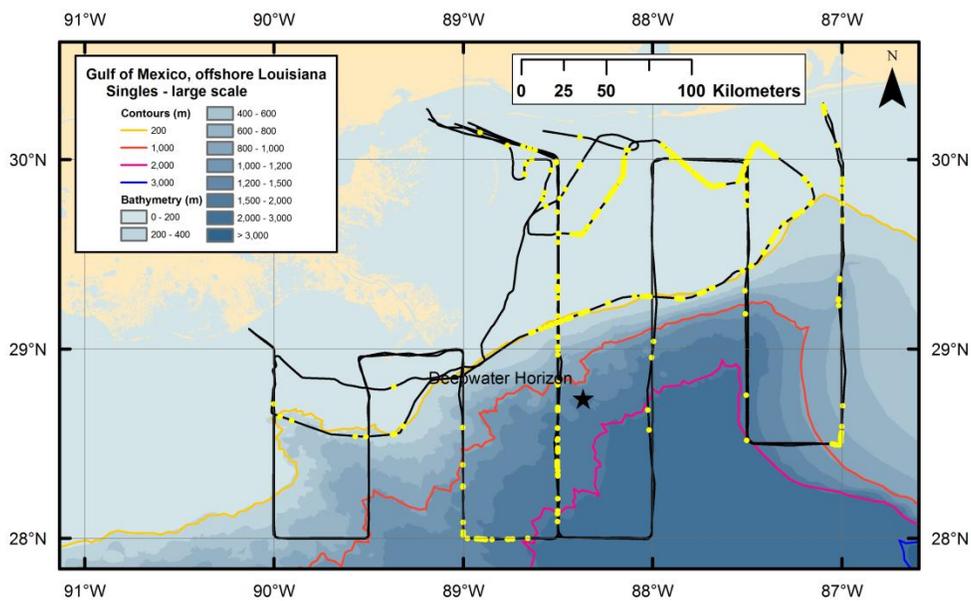
Figure 13. Flight tracks (black lines) and positions of single fish detected during the day (yellow circles), all from the large-scale surveys after the first one and from the search flight.
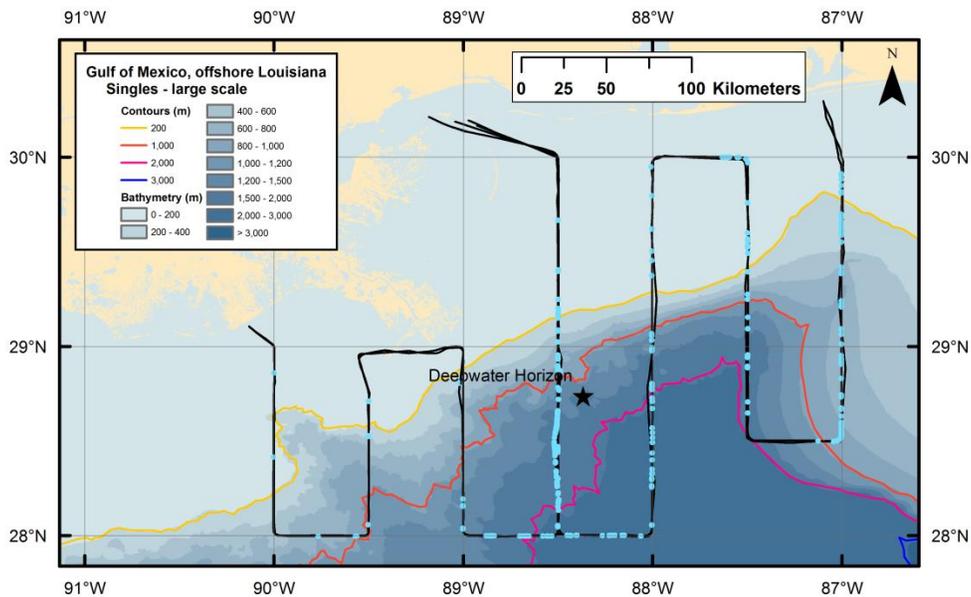
Figure 14. Flight tracks (black lines) and positions of single fish detected at night (blue circles), all from the large-scale surveys after the first one.

A comparison of Figures 9 and 10 suggests diurnal migration of fish to the surface at night in some areas but not in others. This would suggest different targets in some areas, which might have different scattering properties. This led us to calculate the contrast and depolarization if each of the individual fish as described in the methods section.

There was a high degree of correlation between contrast and depolarization ratio, which suggests that both are related to the size of the animal. A larger animal has a larger area and produces a larger return. It also has a rougher surface, which produces greater depolarization. For all of the data, the correlation coefficient was 0.78 with a linear regression of $D = 0.64\, C + 0.38$, where D is the depolarization ratio and C is contrast. For no target, we would expect both D and C to be unity, and the regression produces a value of $D = 1.02$ when $C = 1$, which is very close to the expected result.

It is interesting to consider the largest targets, which we will define as those with $C > 2$. In the initial large-scale survey (Figure 15), the largest concentration of strong returns was at night in the region bounded by 89 and 89.5° W and by 28 and 28.5° N. In other areas where there were high concentrations of single fish, most of these had lower contrast than our threshold value of two. We found that 84% of the high-contrast targets detected during this initial survey were at night, providing strong evidence for diurnal migration of these animals to the surface at night.
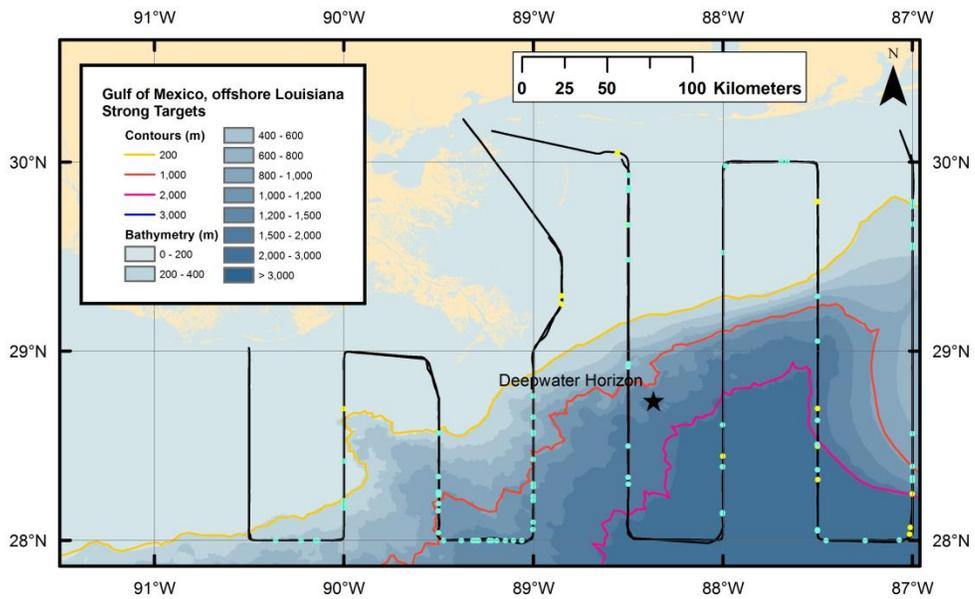
Figure 15. Flight tracks (black lines) and positions of high-contrast single fish detected during the day (yellow circles) and at night (blue circles), all from the initial large-scale survey.

The small-scale surveys (Figure 16) show strong returns that are much more scattered. During the two small-scale surveys on the shelf, only 38% of the strong returns were at night. There seems to be no diurnal migration of strong scatterers in shallow water. If anything, they are slightly deeper at night (average depth 11 m) than during the day (average depth 9 m).
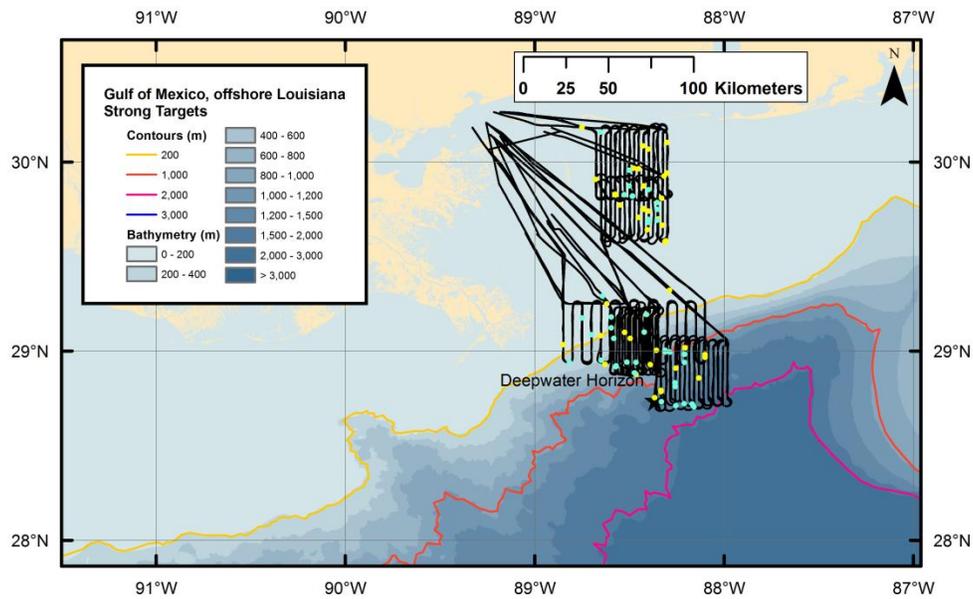
Figure 16. Flight tracks (black lines) and positions of high-contrast single fish detected during the day (yellow circles) and at night (blue circles), all from small-scale surveys.

The other large-scale surveys (Figure 17) produced even fewer high-contrast returns. Neglecting the search pattern, which was only done during the day, evidence of diurnal migration was again observed, although, with 71% of the detections at night, it was not quite as pronounced as during the first large-scale survey. We note that the first survey was conducted very near the dark of the moon. The last large-scale survey was conducted under a ¾ moon, so this may have has an effect.
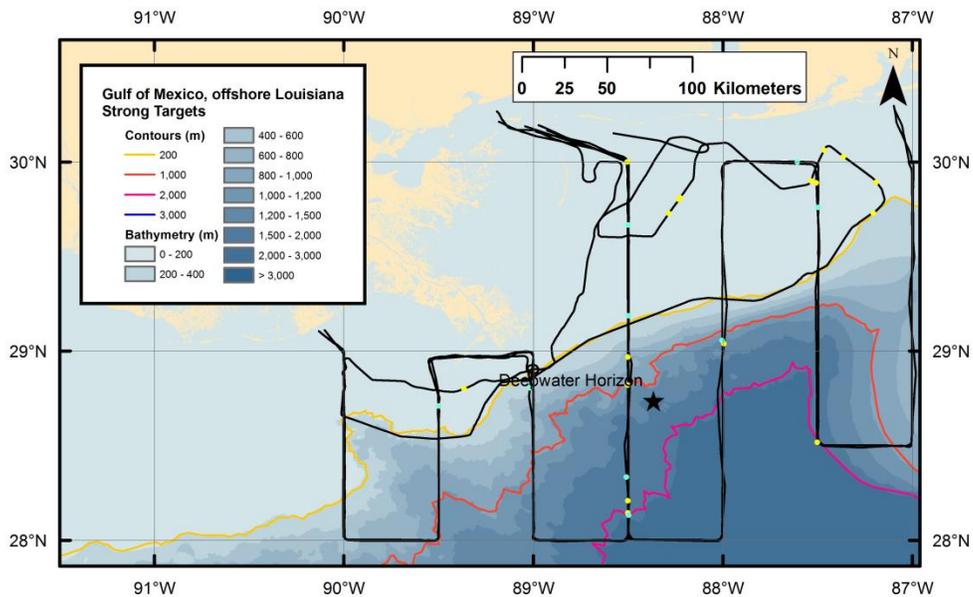
Figure 17. Flight tracks (black lines) and positions of high-contrast single fish detected during the day (yellow circles) and at night (blue circles), all from the large-scale surveys after the first one.

We separated the data into four segments to do some statistical analysis of the high-contrast targets. The four segments were the initial large-scale survey, the small-scale surveys on the shelf, the other small-scale surveys, and the other large-scale surveys. For each segment, we calculated the average longitude of the high-contrast returns, their average latitude, their average daytime and nighttime depths, and the fraction that occurred during the night. The average longitudes were all within a range of about 0.1°, so we can use latitude as a proxy for distance offshore. Two correlations were particularly interesting. The first was a negative correlation (r = -0.97. p = 0.03) between latitude and nighttime fraction. This suggests that diurnal migration becomes more pronounced the farther offshore one goes. The second was a positive correlation (r = 0.99, p = 0.01) between latitude and the nighttime depth of the strong targets. The targets farther offshore were closer to the surface at night than were those closer to the shore.

3.3 Layers

The final return types that were extracted from the data can be characterized as layers. Generally, three different types were observed. Benthic layers were right on the bottom in shallow water, often in depressions. Plumes had one end on the bottom, but the other end rose higher in the water column and sometimes approached the surface. Pelagic layers were horizontal layers not associated with the bottom.   Figure 18 shows an example of a benthic layer and a plume. Note that in both cases, the return from the bottom is reduced by the attenuation through the layer.
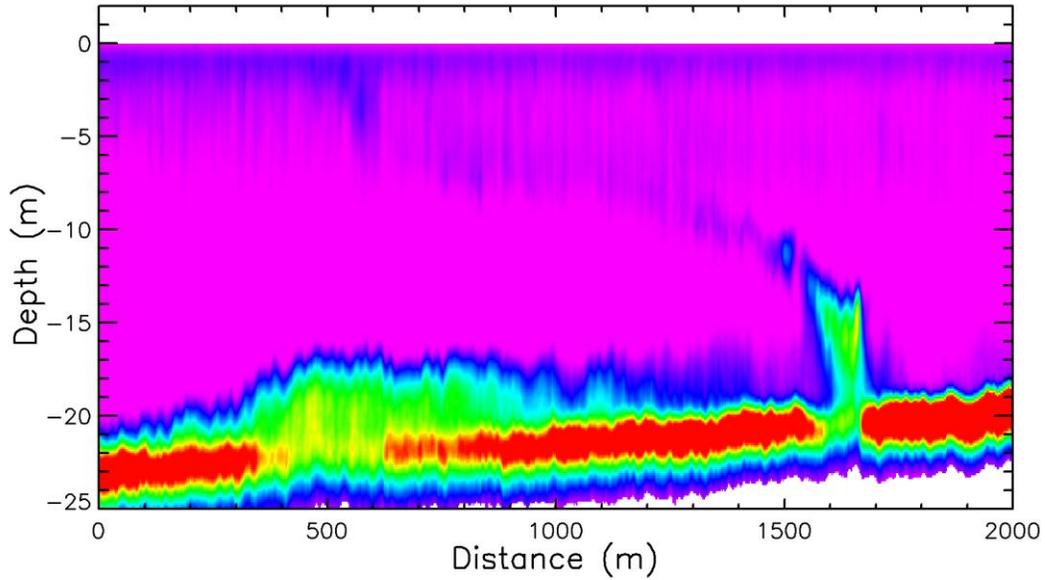
Figure 18. A benthic layer, centered at a distance of 500 m, and a plume, centered at about 1650 m. The bright red band between 20 and 23 m depth is the bottom.

The observed layers seemed to be mostly on the shelf, as seen in Figures 19-21. The observed benthic layers and plumes, of course, were all in shallow water where the LIDAR could penetrate to the bottom. It is tempting to identify plumes like the one in Figure 18 as oil seeps, and the locations will be compared with the locations of known seeps to see if this might be valid.
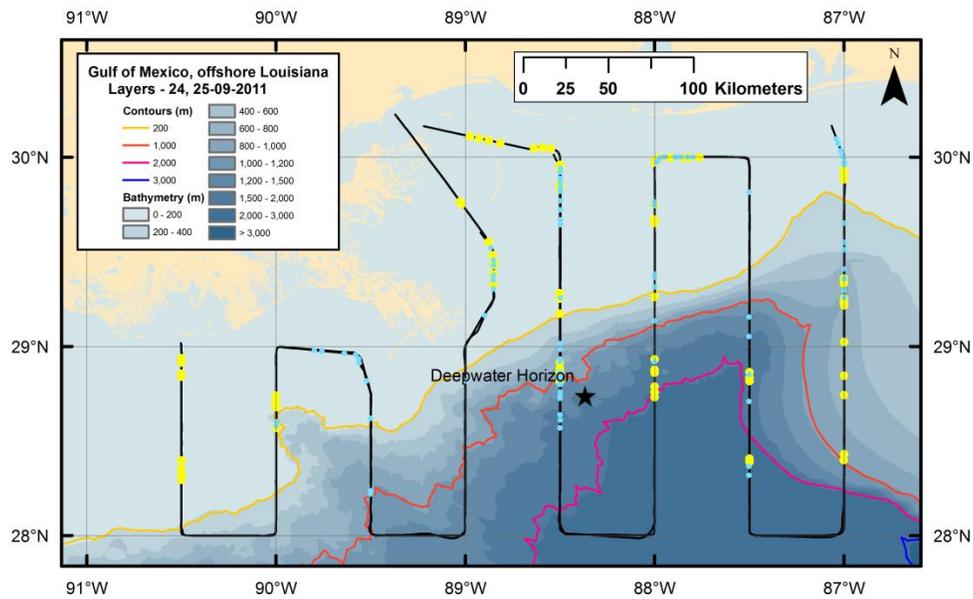
Figure 19. Flight tracks (black lines) and positions of layers detected during the day (yellow circles) and at night (blue circles), all from the initial large-scale survey.
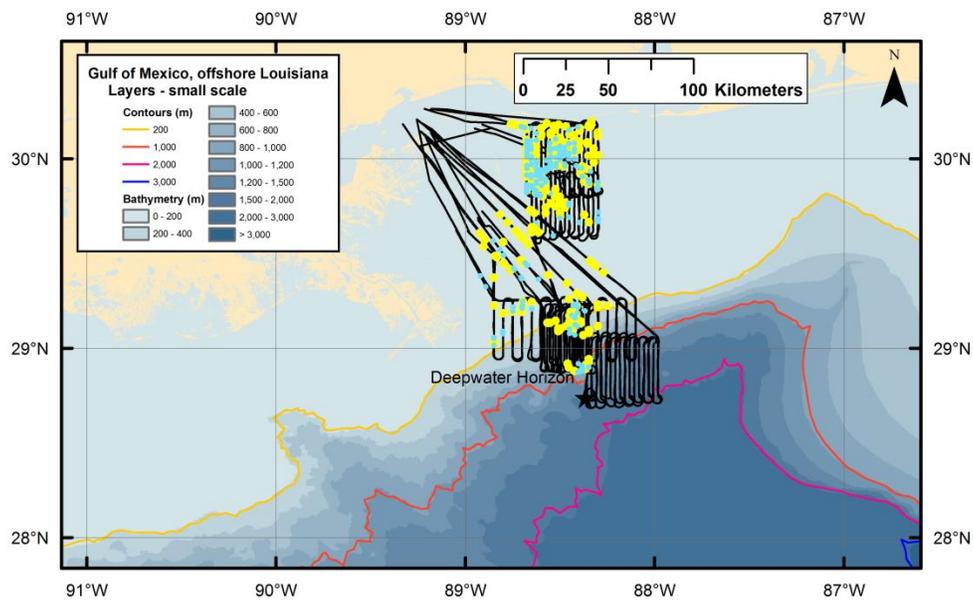
Figure 20. Flight tracks (black lines) and positions of layers detected during the day (yellow circles) and at night (blue circles), all from the five small-scale surveys.
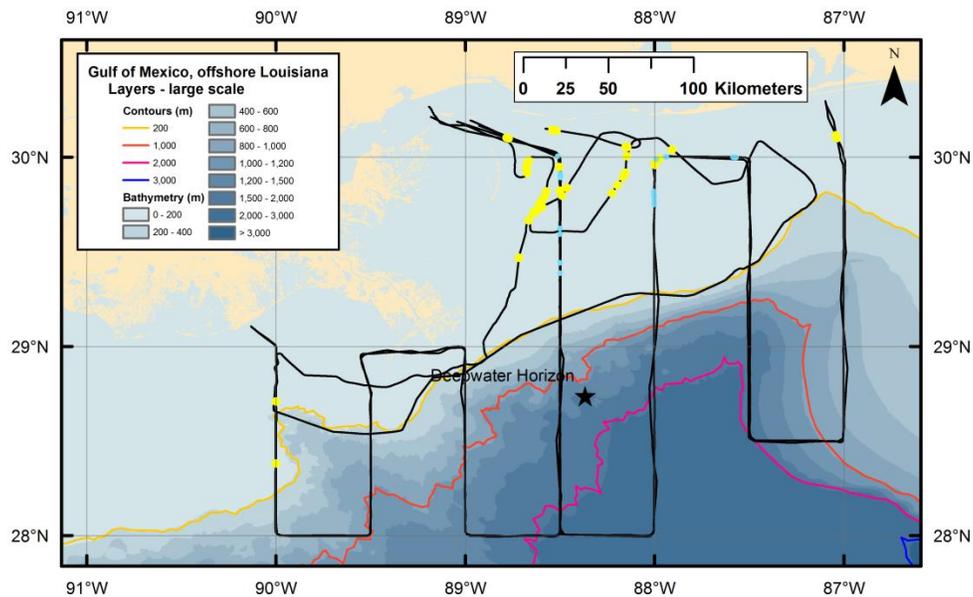
Figure 21. Flight tracks (black lines) and positions of layers detected during the day (yellow circles) and at night (blue circles), all from the large-scale surveys after the first one and from the search flight.

3.4 Penetration Depth

The utility of the LIDAR, of course, depends on how much of the water column it is able to penetrate. This depends on water clarity and is greater in offshore waters than in the Mississippi River plume. The penetration depth for the first large-scale survey (Figure 22) clearly shows the river plume, where the penetration is less than 20 m. Much of the shelf region has a penetration depth of 20 – 30 m and much of the region offshore is greater than 30 m. Nighttime penetration is slightly better, but the pattern is about the same.
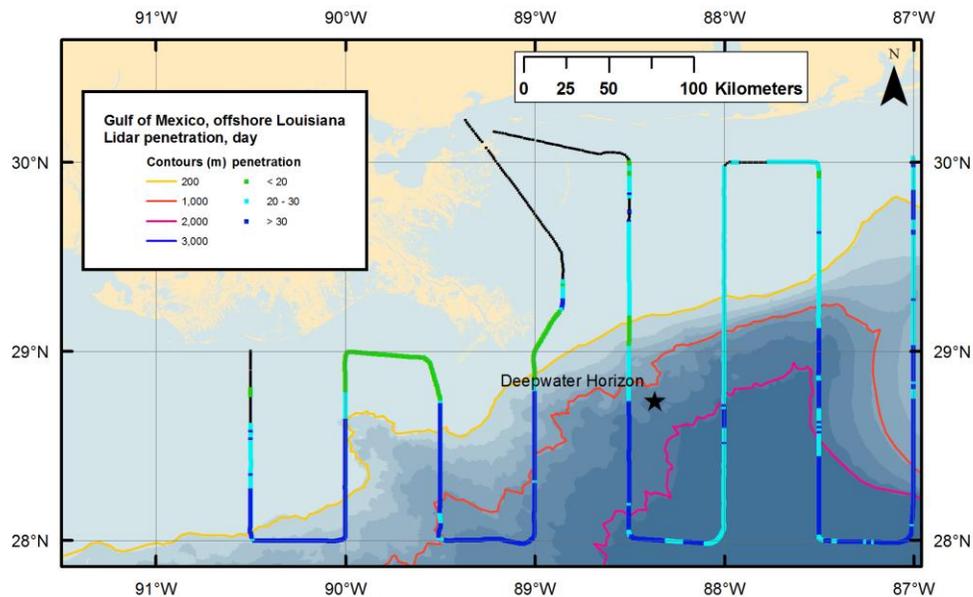
Figure 22. Daytime LIDAR penetration depth for the first large-scale survey. Black lines are where the LIDAR was seeing clear to the bottom.

4   SUMMARY

It is convenient to summarize the LIDAR results in terms of the original objectives. The fifth objective relates to the data from the surface vessel, so only the first four are considered.

a)   Document the large scale distribution of epipelagic fish and plankton in the study area.

Fish schools and layers were generally found on the shelf. Conversely, single fish targets were found more often offshore. East to west, the most active area was near the center of the study area, between 88° and 89° W. All of the small-scale surveys were in this area. There were significant changes in the large-scale distribution during the survey period. For example, the number of schools in the eastern region decreased only slightly, but there was a huge decrease in the number of single fish and of layers.

b)   Document day/night differences in the distribution of fish and plankton.

We did not see the dramatic day/night differences that we have seen in some surveys, but there were differences. In the first large-scale survey and in all of the small-scale shelf surveys, there were more schools detected during the day than at night. Conversely, there were more schools detected at night than during the day in subsequent large-scale surveys and in small-scale surveys over the slope and offshore. There were more single targets detected at night than during the day except for the small-scale surveys over the shelf and over the slope. Except for the first small-scale survey over the shelf, there were more layers detected at night than during the day. Some of this change might be explained

22

by pelagic fish changed their configuration from dense schools during the day to more diffuse layers at night. Comparison of the LIDAR data with surface data should answer this question.

c)   Investigate spatial scales not available to the ship survey.

In two days, the aircraft was able to cover the region between 87° and 90.5° W out to 28° N with a resolution of 0.5° of longitude both day and night (2300 nmi of survey track). This would take a ship almost 10 days of constant steaming at 10 kts, and we have demonstrated that the distribution of fish in the region changed on this time scale. On the small scales, we made several surveys over 10 nmi square regions with 0.75 nmi transect spacing.

d)   Use aerial imagery/LIDAR to direct ship sampling to regions of high biological concentrations.

Several times during the surveys, the surface vessel was directed to regions where the LIDAR was detecting high levels of biological return. These will be used to help identify the identity of the LIDAR targets when the surface data become available.

A. DATA FORMAT APPENDIX

The raw lidar data files are in a ".png" gray-scale image format that is 2000 pixels by 2200 pixels. Each column in the image represents a single lidar shot, so each data file represents about 67 seconds at the lidar repetition rate of 30 Hz. The first 1000 pixels in each column are the 1000 samples of the co-polarized receiver channel. The digitizer has eight bits, so there are 256 levels of gray. The next 1000 pixels are the simultaneous samples from the cross-polarized receiver. The last 200 samples are used to record ancillary information in ASCII format. This information includes (in order): latitude (decimal degrees), longitude, N (for north latitude), W (for west longitude), co-polarized receiver gain, cross-polarized receiver gain, voltage on a cutoff switch, voltage from the pitch sensor, voltage from a sea-surface temperature radiometer, space for an additional sensor (currently unused), date, and time. File naming convention is FL11*dddhhmmss*.png, where *ddd* is year day, *hh* is hour, *mm* is minute, and *ss* is second. These describe the time the file was created (UTC).
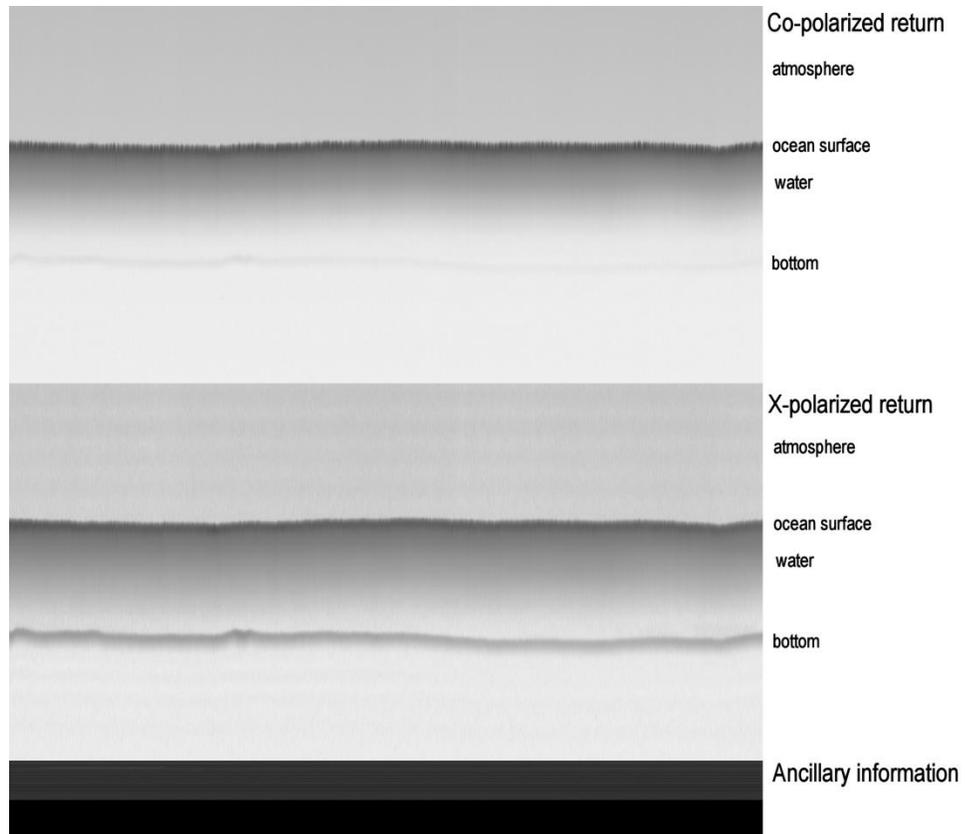
Figure A1. Sample of raw data file showing the co-polarized return at the top, the cross-polarized return lower down, and the ancillary information at the bottom. The lidar returns from that atmosphere, the ocean surface, the water, and the bottom of the ocean are can be seen in both polarizations.

The video files are ".wmv" Windows Media Video files. Date and time are on the screen.

The processed data are organized into three Excel workbooks for schools, singles, and layers, respectively. Each workbook has a spreadsheet for each day. The spreadsheet columns are labeled as in Table A1 – A3, which also includes a brief description of each parameter. As described in the text, only the cross-polarized return was used in this processing. Note that signal strength is expressed in terms of the photocathode current. This has been corrected for attenuation in the water, so can be converted to volume backscatter coefficient by the application of a single calibration coefficient.

Table A1. Processed-data parameters for schools detected by the lidar.

Parameter	Description
time	decimal hours, UTC
lon	decimal degrees
lat	decimal degrees
length	m
depth	m
penetration_depth	extent of lidar penetration (m)
strength	average signal at photocathode (A)
shot1	shot number of start of school
shot2	shot number at end of school
top_sample	sample number at top of school
bot_sample	sample number at bottom of school
file	raw file name
number	number of file within data directory

Table A2. Processed-data parameters for single targets detected by the lidar.

Parameter	Description
time	decimal hours, UTC
lon	decimal degrees
lat	decimal degrees
depth	m
strength	signal at photocathode, A
file	raw data file name
number	number of file within data directory
shot	shot number within file

Table A3. Processed-data parameters for layers and plumes detected by the lidar.

Parameter	Description
time	decimal hours, UTC
lon1	start of layer, decimal degrees
lat1	start of layer, decimal degrees
depth1	start of layer, m
lon2	end of layer, decimal degrees
lat2	end of layer, decimal degrees
depth2	end of layer, m
file	raw data file name
number	number of file within data directory
shot1	starting shot number within file
shot2	ending shot number within file

5   REFERENCES

Brown, E. D., J. H. Churnside, et al. (2002). "Remote sensing of capelin and other biological features in the North Pacific using lidar and video technology." Ices Journal of Marine Science **59**(5): 1120-1130.

Carrera, P., J. H. Churnside, et al. (2006). "Comparison of airborne lidar with echosounders: a case study in the coastal Atlantic waters of southern Europe." Ices Journal of Marine Science **63**(9): 1736-1750.

Churnside, J. H. (2008). "Polarization effects on oceanographic lidar." Optics Express **16**(2): 1196-1207.

Churnside, J. H., D. A. Demer, et al. (2009). "Comparisons of Lidar, Acoustic and Trawl Data on Two Scales in the Northeast Pacific Ocean." California Cooperative Oceanic Fisheries Investigations Reports **50**: 118-122.

Churnside, J. H., D. A. Demer, et al. (2003). "A comparison of lidar and echosounder measurements of fish schools in the Gulf of Mexico." Ices Journal of Marine Science **60**(1): 147-154.

Churnside, J. H. and P. L. Donaghay (2009). "Thin scattering layers observed by airborne lidar." Ices Journal of Marine Science **66**(4): 778-789.

Churnside, J. H., A. F. Sharov, et al. (2011). "Aerial surveys of fish in estuaries: a case study in Chesapeake Bay." Ices Journal of Marine Science **68**(1): 239-244.

Churnside, J. H., E. Tenningen, et al. (2009). "Comparison of data-processing algorithms for the lidar detection of mackerel in the Norwegian Sea." Ices Journal of Marine Science **66**(6): 1023-1028.

Churnside, J. H. and R. E. Thorne (2005). "Comparison of airborne lidar measurements with 420 kHz echo-sounder measurements of zooplankton." Applied Optics **44**(26): 5504-5511.

Churnside, J. H. and J. J. Wilson (2001). "Airborne lidar for fisheries applications." Optical Engineering **40**(3): 406-414.

Churnside, J. H. and J. J. Wilson (2004). "Airborne lidar imaging of salmon." Applied Optics **43**(6): 1416-1424.

Reese, D. C., R. T. O'Malley, et al. (2011). "Epipelagic fish distributions in relation to thermal fronts in a coastal upwelling system using high-resolution remote-sensing techniques." ICES Journal of Marine Science: Journal du Conseil **68**(9): 1865-1874.

Tenningen, E., J. H. Churnside, et al. (2006). "Lidar target-strength measurements on Northeast Atlantic mackerel (Scomber scombrus)." <u>Ices Journal of Marine Science</u> **63**(4): 677-682.

Zorn, H. M., J. H. Churnside, et al. (2000). "Laser safety thresholds for cetaceans and pinnipeds." <u>Marine Mammal Science</u> **16**(1): 186-200.